NASA
Technical
Paper
2406

C.2

AVSCOM
Technical
Report
84-C-17

December 1984

High-Temperature Erosion of Plasma-Sprayed, Yttria-Stabilized Zirconia in a Simulated Turbine Environment

Robert F. Handschuh

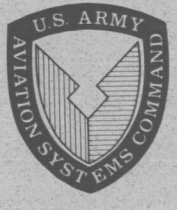

NASA

NASA Technical Paper 2406

AVSCOM Technical Report 84-C-17

1984

High-Temperature Erosion of Plasma-Sprayed, Yttria-Stabilized Zirconia in a Simulated Turbine Environment

Robert F. Handschuh

Propulsion Laboratory
USAAVSCOM Research and Technology Laboratories
Lewis Research Center
Cleveland, Ohio

National Aeronautics and Space Administration

Scientific and Technical Information Branch

Summary

The high-temperature erosion of blade tip seals that can occur in gas turbine engines was simulated by using a modified jet fuel combustor. The erosion resistance of engine seal specimens formed from plasma-sprayed, yttria-stabilized zirconia (YSZ) was evaluated at three impingement angles (20°, 45°, and 90° (perpendicular to the flow)) and at three locations downstream of the nozzle (7.6, 10.2, and 12.7 cm (3, 4, and 5 in.) from the nozzle exit to the center of the specimen surface). Tests were also performed to evaluate the following test rig parameters: particle velocity (260 to 320 m/s; 850 to 1050 ft/s), particle diffusion in the hot gas flow, and specimen surface temperature (1250 to 1600 °C; 2280 to 2900 °F).

The 19 seal specimens tested were formed of two different weight percentages of Y_2O_3 and two different compliant layer materials (Brunswick Co. FM-534 and H-875). Neither of these specimen differences had any noticeable effect on erosion rate. The series of erosion tests showed that surface imperfections are zones of increased erosion activity and that the rate of material removal strongly depended on the impingement angle. Erosion proceeded much more slowly at 20° than at 45° or 90°. Some specimens examined, after testing, with a scanning electron microscope showed plastic deformation although the specimen weight loss data indicated a brittle material erosion process. Overall surface appearance, observed with SEM, changed depending on the impingement angle during the erosive process. Surfaces examined at 90° impingement exhibited random edge and side impacts, but at 45° and 20° impingements the impacts were oriented in the direction of the combustion gas flow.

Introduction

The major emphasis in gas turbine research has been on improving efficiency. This can be done by decreasing clearances between the turbine rotor and the turbine tip seals and reducing cooling requirements while increasing gas path temperatures and turbine rotating speeds. Therefore degradation of tight clearances and damage to airfoils, rotating and stationary, are of the utmost importance (ref. 1).

Loss of performance can occur in many forms under the environmental conditions found in gas turbines. The degradation of materials due to solid particle erosion at high temperatures is one of these forms. Erosion damage can be caused by ingested airborne particles, normal engine wear, and products of combustion. The environment in a gas turbine is conducive for the erosion process to proceed. Because gas temperatures are high, material properties diminish. The high gas velocity allows particles to attain sufficient kinetic energy to damage engine components.

Removal of material by erosive processes in a commercial gas turbine is typically a long-term problem. However, certain operating conditions can result in large amounts of debris being ingested in a short time. Several thousand hours of normal erosive wear may be accumulated in just a few moments.

The present study investigated high-temperature erosion rig parameters and tested plasma-sprayed, yttria-stabilized zirconia (YSZ) seal specimens. Test rig parameters such as particle velocity, particle pattern diffusion in the high-temperature gas flows, and attainable specimen surface temperatures were experimentally calibrated. Specimens simulating turbine tip shroud seals, where the exposed surface that was eroded was the YSZ, were tested at three impingement angles and at three positions downstream of the nozzle exit plane. Each specimen was typically tested repeatedly at only one location and one angle of impingement. Erosion results are presented as specimen weight loss versus particles used (mass of particles injected into the combustor flow).

Test Rig Configuration

The test rig consisted of a jet fuel combustor modified so that the erosive grit material (aluminum oxide) could be injected into the centerline of the combustor (fig. 1). Combustion air was provided by 827-kPa (120-psi) shop air and preheated before being mixed with the jet fuel. The burning of the fuel in the combustor provided the test rig with a high-temperature and gas-velocity source. The erosive material was dispensed into a carrier gas tube by a commercially available powder feed mechanism. The erosive grit and carrier air were preheated before injection into the combustor. The specimen was located

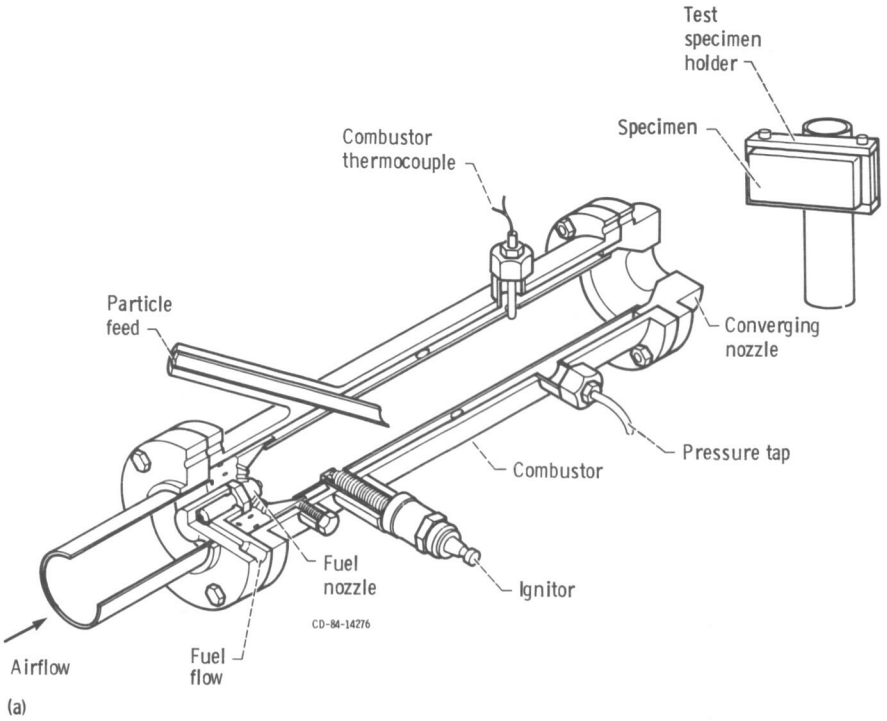

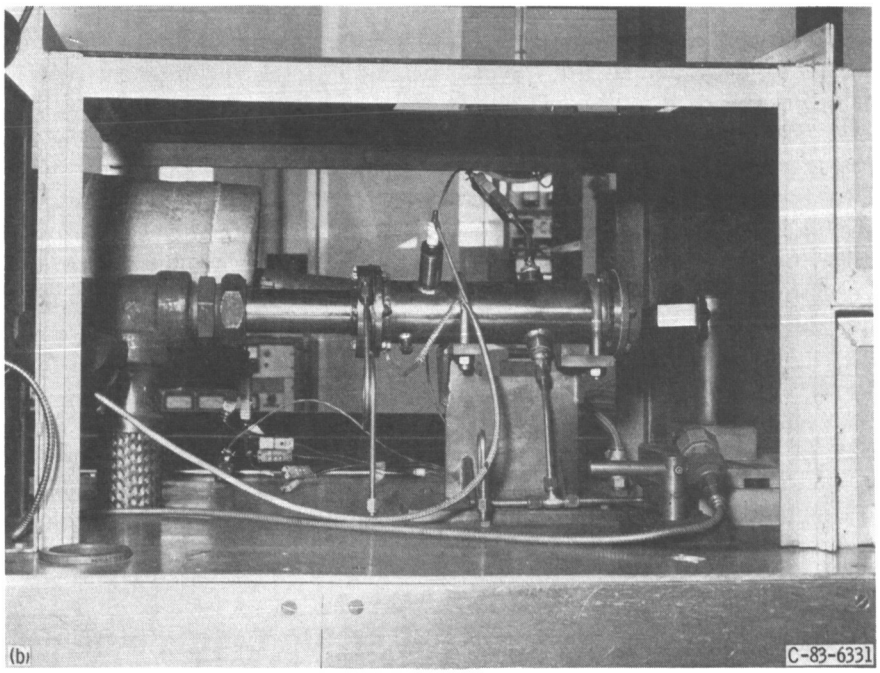

(a) Cutaway view.
(b) Test installation.

Figure 1.—High-temperature erosion rig.

downstream of the nozzle exit and positioned in the flow at a location to provide the test-required specimen surface temperature conditions and at an impingement angle of interest.

The test rig had a converging nozzle and sonic velocity was maintained during the entire test procedure. This provided the particles with as high an accelerating environment as possible for the design of the test rig while minimizing the amount of diffusion of the erosive grit material downstream of the nozzle exit. An alternative design of high-temperature erosion test facilities employs long vertical acceleration tubes to allow particles and carrier gas velocities to become essentially the same (ref. 2). This is useful in studying how particle velocity

influences the erosion process. However, this design typically cannot produce high-temperature test conditions because of the amount of heat lost to the long acceleration section.

Present gas turbine temperatures are in the 1300 °C (2400 °F) range, and the trend is toward higher temperatures to achieve thermal efficiency payoffs. Meaningful tests of gas path seal materials require evaluation at these higher temperatures to determine their erosive characteristics.

Another aspect of the test rig is that the specimen can be cooled on the substrate side to allow simulation of heat flux through the specimen. In the typical gas turbine, cooling air to the gas path seals is bled off from the compressor. This air is used to cool the back side of the seal as well as to provide a positive pressure drop of compressed air to counteract any chance of hot combustion gas backflowing around the seal.

Downstream of the test section the spent grit material and other debris are collected in a water mist scrubber and then discharged to the vent.

Instrumentation

Instrumentation on the test rig monitored temperature, pressure, and flow conditions during the tests. These data were taken and averaged by a minicomputer during the tests. The instrumentation used to control rig set points was essential to repeatable test results. One set of pressure and flow conditions were chosen. Tests for calibration and operation were conducted under the same conditions.

Specimen instrumentation was only concerned with monitoring temperatures during the test procedure. Each specimen was thermocoupled at two locations at the interface between the substrate and test surface material and at two locations on the back side of the substrate (fig. 2). Surface temperatures were monitored by an optical pyrometer[1] and a thermography system[2] thermally mapped the surface. The amount of surface that the pyrometer used to determine the surface temperature was approximately 5.1 cm^2 (0.8 in^2). The thermography system was used to investigate temperature distribution across the specimen. The system has a sensor that is sensitive to radiation in the 8- to 12-μm wavelength range. Since the system must view the specimen through combustion gases, a 10.6-μm filter was used to eliminate combustion product radiation.

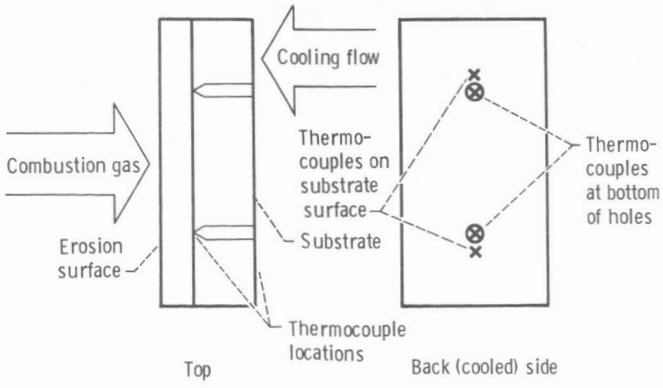

Figure 2.—Typical high-temperature erosion test specimen with locations of instrumentation.

High-Temperature Erosion Parameter Calibration

Before testing it was important to have the test process variables for the test facility investigated. Experiments were performed to gather the necessary information on specimen surface temperatures and thermal gradients, particle velocity, and particle pattern diffusion in the flow as a function of specimen location.

Specimen Surface Temperature and Thermal Gradients

When testing turbine materials in a high-temperature erosive medium, it is desirable to have the target surface attain a temperature representative of turbine environments. Surface temperatures are affected by the distance downstream from the nozzle exit, the angle of impingement, the additional flows in the combustor due to particle carrier gas injection, and the grit material itself.

Surface temperature as a function of impingement angle and distance downstream was investigated by using test specimen 10a (table I). The results of the series of tests (fig. 3) indicate that attainable surface temperature for the test hardware configuration depended strongly on impingement angle and downstream distance.

For each location and incidence angle the rig was ignited and brought up to steady-state rig set points as quickly as possible. Once temperatures stabilized, in approximately 5 min, the additional carrier gas was allowed to flow through the particle feed system. This provided a simulation of all airflow conditions without introducing the grit material in the flow. The additional airflow through the particle feed system produced at most a 25 deg C (45 deg F) drop from the surface temperature when the carrier gas was turned on.

During erosion tests, when the erosive grit material and extra air are injected into the combustion flow, the surface temperature can drop 90 to 120 deg C (160 to 220 deg F). Similar losses of surface temperature were

[1]Capintec Instruments, Inc.
[2]Inframetrics, Inc.

TABLE I.—TEST SPECIMEN CONFIGURATION

Impingement angle, deg	Distance from nozzle exit to specimen center		Dimensions of plasma-sprayed layer				Y_2O_3 content, wt%	Compliant layer type[a]	Specimen
			YSZ		NiCrAlY (bond coat)				
	cm	in.	mm	mil	mm	mil			
90	7.6	3	2.06	81	0.10	4	8	H-875	10a
	10.2	4	2.11	83	.10	4	8	FM-534	1a
	10.2	4	1.60	63	.08	8	8	↓	16
	10.2	4	1.93	76	.13	5	12	↓	10
	12.7	5	2.13	84	.08	3	8	↓	2a
	12.7	5	2.08	82	.10	4	↓	H-875	5a
	12.7	5	1.70	67	.15	6	↓	FM-534	24
45	7.6	3	2.03	80	.08	3	↓	H-875	9a
	7.6	3	1.60	63	.10	4	↓	FM-534	14
	10.2	4	1.88	74	.10	4	12	FM-534	11
	10.2	4	1.80	71	.13	5	12	FM-534	12
	12.7	5	2.06	81	.10	4	8	H-875	11a
	12.7	5	1.73	68	↓	↓	↓	FM-534	7
20	7.6	3	2.03	80	↓	↓	↓	H-875	7a
	7.6	3	2.08	82	↓	↓	↓	H-875	8a
	10.2	4	2.08	82	↓	↓	↓	FM-423	4a
	10.2	4	2.11	83	.08	3	↓	H-875	12a
	12.7	5	2.13	84	.10	4	↓	FM-534	3a
	12.7	5	2.06	81	.08	3	↓	H-875	6a
Used in preliminary calibration tests			1.85	73	.13	5	12	FM-534	9

[a]Brunswick Corporation.

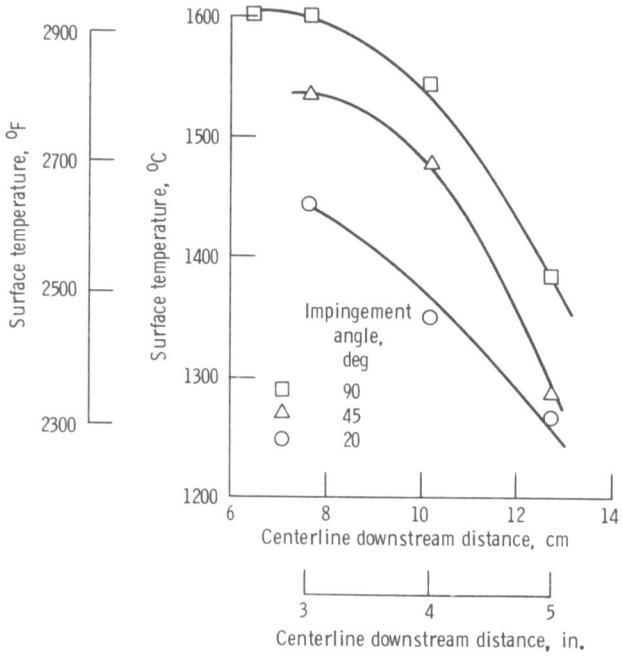

Figure 3.—Attainable steady-state surface temperature. (Data taken from sample 10a. Surface temperature during erosion would be 90 to 120 deg C (160 to 220 deg F) lower for grit flow of 0.2 g/s (1.6 lb/hr).)

recorded for all locations and impingement angles. Only a 25 deg C (45 deg F) loss is accounted for by the excess air from the particle feed system. Apparently the erosive grit material was responsible for extracting energy from the combustion products. A typical specimen test temperature history during an erosion test cycle is shown in figure 4.

It is conceivable that removal of material by any process is associated with increases in temperature because energy is dissipated in the form of heat. However, this was not found, as indicated by the instrumentation, and is thought to be masked in the net sum of temperature loss due to particles gaining heat from the flow.

Knowing the emittance of YSZ, it was possible to determine the temperature changes directly from the video monitor. (In ref. 3 plasma-sprayed coatings of YSZ with thicknesses greater that 510 μm (0.020 in.) were shown to have emittances nearly equal to 1.0 in the 8- to 12-μm wavelength range.) An example of a typical thermal image when a YSZ specimen had reached steady-state temperature is shown in figure 5.

The temperature dependence of the specimen on location downstream, impingement angle, and changes in combustor conditions during testing is governed by a very

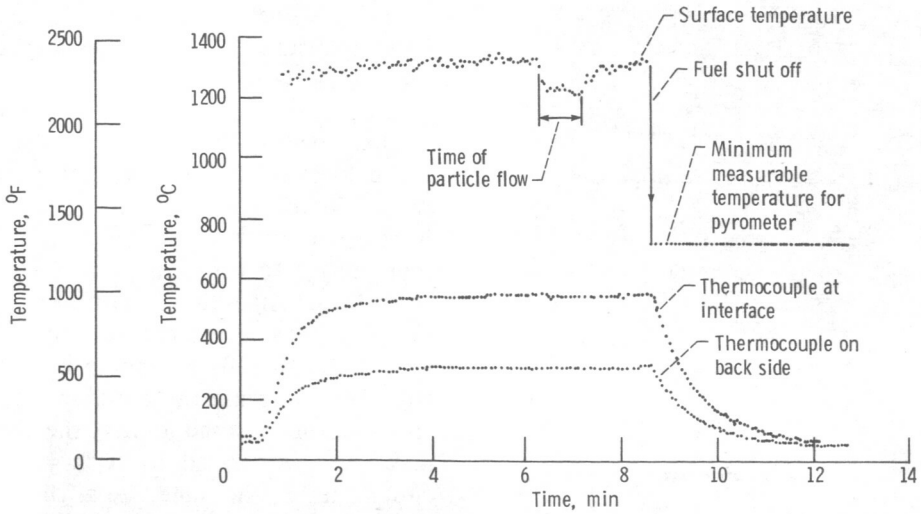

Figure 4.—Temperature-time history of a typical erosion test. Data presented are for sixth test of sample 3a at 12.7 cm (5 in.) downstream of nozzle exit and 20° impingement angle.

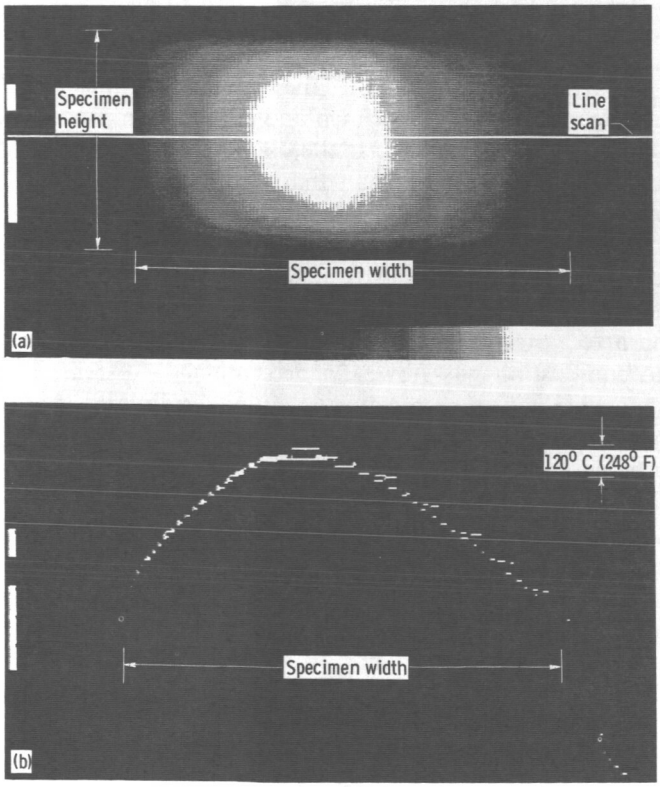

(a) Thermal image of YSZ specimen.
(b) Thermal profile of YSZ specimen from line scan location shown in fig. 5(a).

Figure 5.—Thermography image and temperature profile across specimen. Sample at 10.2 cm (4 in.) downstream of nozzle exit and 90° impingement angle. Surface temperature difference from center to edge, approximately 480 deg C (860 deg F); pyrometer temperature, 1540 °C (2800 °F).

complex heat transfer situation. Radiation between the specimen surface and the high-temperature combustion products, the nozzle surfaces, and the surroundings of the specimen along with the forced-convection terms all contribute to determining the surface temperature for a particular location and impingement angle. The solution of a complex problem such as this, while an interesting topic, was not the focus of this study. It was decided that it would be more expedient to measure the temperature variation and not try to model it.

Particle Type, Size, and Velocity

The erosion material chosen for this series of high-temperature erosion experiments was aluminum oxide. This material is used for many grinding applications. Its abrasive qualities, high melting temperature, and hardness make it a suitable grit material for studying high-temperature solid particle erosion (fig. 6).

The aluminum oxide grit material used for testing was 130 μm (0.005 in.) in average diameter. Grit material was sieved twice to further narrow the distribution of particle size. Particles used in the test program had to pass through a sieve with a 149-μm mesh opening but not through a sieve that had a 104-μm mesh opening.

Particles of this size were used for two reasons. First, particles with average diameters greater than 100 μm are minimally affected by secondary flows around the specimen (ref. 4). Thus the particle-gas flow that impinges on the specimen will cause erosion damage and will not tend to deviate from impacting the surfaces because of the flow over these surfaces. The second reason was the experimental determination of particle

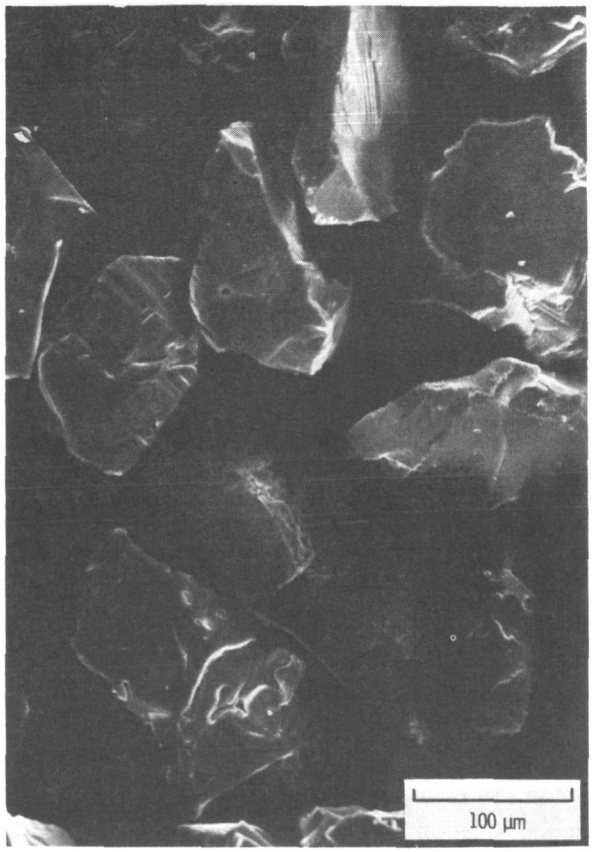

Figure 6.—Aluminum oxide grit material used in high-temperature erosion studies, showing sharp edges and irregular shape.

velocities. Because of the method used to determine particle velocities, particles of this size would be less affected by abruptly changing flows.

Particle velocity in gas flows can be measured by several methods. These methods include laser Doppler anemometry, high-speed photography, or a double-disk time-of-flight method. The accuracy of each method is proportional to funds expended for instrumentation and investigators' time (ref. 5). As mentioned, the need for this measurement can be avoided by using long vertical acceleration tubes that allow the particles to have sufficient time to reach the gas flow velocity (ref. 1).

In this study the particle velocity of the grit material was experimentally determined by a double-disk system (ref. 6). Two parallel disks were rotated on an axis parallel to the high-temperature gas flow (fig. 7). Circular holes in the first disk allowed the gas and particle flow to pass between the two disks. The angular difference between the initial center position of the hole and the erosion pattern center provided the necessary information. The hole position in the upstream disk was referenced on the target disk by pinning the two disks together. The disks were separated by blocks of the same length at 90° increments to keep the distance between the disks constant. During the velocity test the disk assembly's angular speed was monitored with a strobe light to ensure that the proper average speed measured during the flow of particles was used for calculating velocity.

This method of measuring particle velocity has difficulties. Because the particle velocity was 260 to 320 m/s (850 to 1050 ft/s), the deviation of the particle impact pattern was quite small. Thus the test results are more prone to errors than if there were large pattern centerline changes (lower particle velocity). Initial efforts produced displacements too small to be measured accurately; therefore a number of changes were made (fig. 7) to increase the accuracy of the tests. A higher speed motor was used to drive the disk assembly, and the disks were separated by a larger distance. Also two circular holes (the same size as the nozzle exit diameter) were made in the first disk. Data from both hole locations were used for each test position investigated to find an average velocity for that test. Even on the same test there were data variations of 10 to 15 percent.

Particle Pattern Diffusion in the Flow

Particle interaction with the gas flow must be investigated when the specimen and combustion product stream are similar in size. If the diameter of the test rig nozzle is much smaller than that of the specimen, the problem is at least partially avoided.

When particles are introduced into the combustion products, they follow approximately the flow streamlines of the diverging high-temperature jet. Thus sample size can affect the erosion rate at any particular location in the combustion gas flow. To determine the extent of divergence of the erosive medium, stainless steel specimens were used with dimensions far in excess of the divergence of the combustion gas–erosive grit flow. Tests were run at positions where test hardware would be evaluated. Rig set points were duplicated, as would occur in an actual test. The samples used were 10 by 10 cm (4 by 4 in.) on the sides by 1 cm (0.25 in.) thick. Particle flow lasted typically 5 minutes and approximately 50 g of grit material was used.

These tests were evaluated by examining the erosion pit. Two downstream locations in the combustion products are discussed here: 7.6 cm (3 in.) and 12.7 cm (5 in.) downstream of the nozzle exit plane—the centerline position extremes where YSZ test hardware was eroded. The pit profiles were measured by passing the sample under a laser profilometer.[3] The system consisted of a low-powered helium-neon laser and a one-dimensional linear diode array. Laser spot position changes on the linear diode array were related to surface height changes. Nonlinearities were eliminated by an

[3]Sigma Research, Inc.

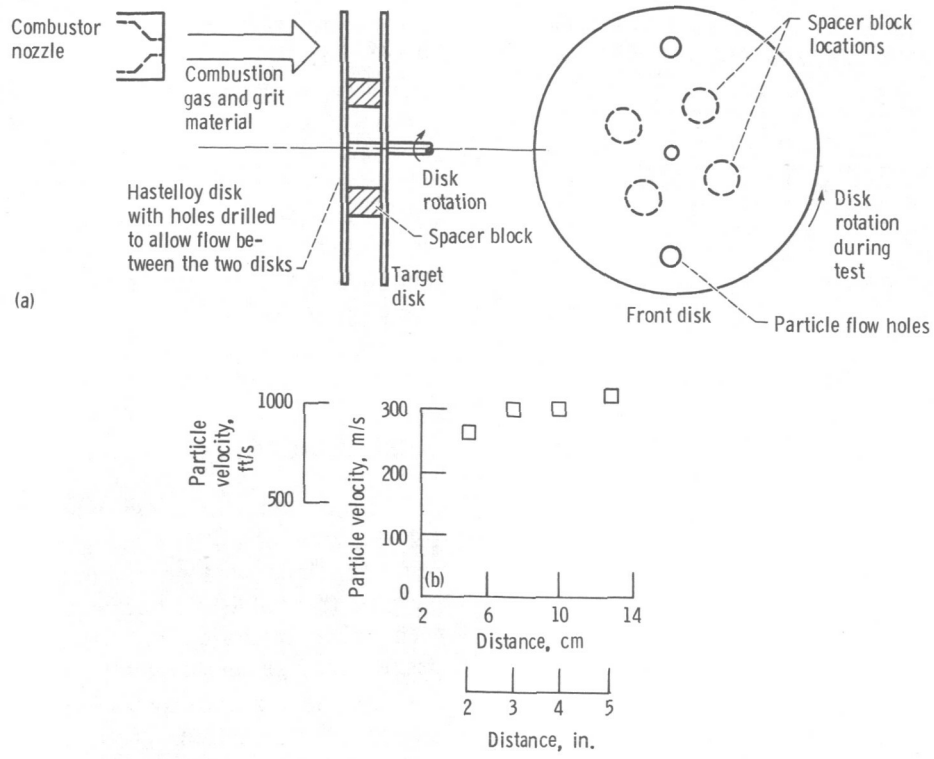

(a) Particle velocity measurement test setup.
(b) Distance from nozzle exit plane to mid-distance between disks.

Figure 7.—Particle velocity measurement test setup and measured results as a function of distance from nozzle exit plane.

internal microprocessor, and the analog output was read by a minicomputer.

A major advantage of the laser profilometer is that its range is greater than 0.76 cm (0.3 in.). Typical highly sensitive surface-contacting profilometers can tolerate height changes of only a few thousands of an inch. The disadvantage is that the laser spot size (0.2 cm; 0.08 in.) does not allow very fine details of surface damage to be measured for this particular laser profilometer system.

A sample surface profile was generated by taking 75 data points at 0.1-cm (0.04-in.) increments with a lead-screw-driven slide. For each location of interest a graph of material removed versus distance across sample was constructed (fig. 8). After taking a number of these plots in the horizontal and then vertical directions an erosion pit map at each downstream location (7.6 and 12.7 cm; 3 and 5 in.) was constructed. The maps (fig. 9) were produced by taking the horizontal and vertical profiles and locating where 0.013 cm (0.005 in.) of damage started. The starting and ending locations were then positioned on a figure of equal size to that of the particle test specimen. The smallest circular area that included all of the data is shown in figure 9. What can be seen from the figure is that the particle centerline does not correspond to the combustion nozzle centerline and also changes with respect to downstream position in the flow.

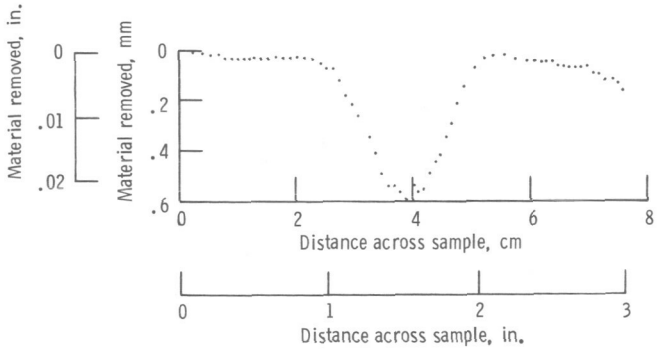

Figure 8.—Surface profile of erosion pit from particle-diffusion-in-flow test. (Data taken at 7.6-cm (3-in.) position on horizontal centerline.)

Specimen Configuration

Specimens for this series of tests consisted of four layers (fig. 10). The base or substrate material was stainless steel. The substrate had two holes drilled almost to the opposite face to allow thermocouple measurements at the higher temperature side of the substrate. Also, two more thermocouples on the back surface provided temperature changes across the specimen substrate.

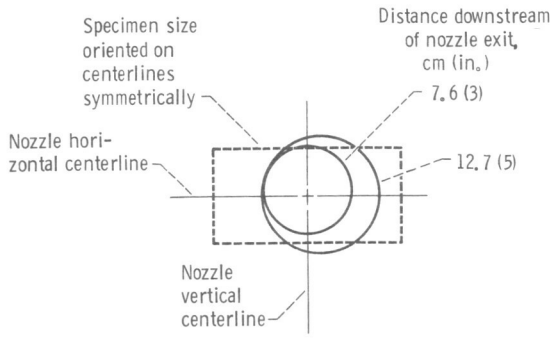

Figure 9.—Particle diffusion patterns at two locations downstream of nozzle and relationship between pattern size and specimen size. (Particle patterns based on where profilometer indicated 0.13 mm (0.005 in.) of surface removed.)

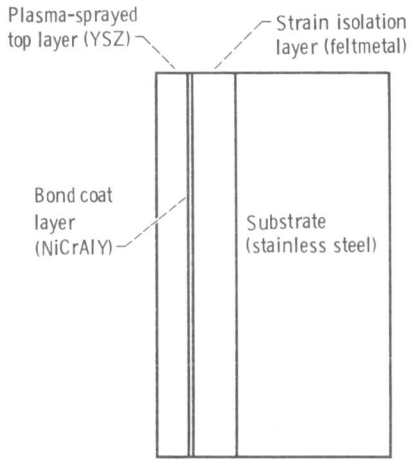

Figure 10.—Typical test rig specimen, showing orientation of material layers used.

The second layer, a fibermetal (compliant) layer, was furnace brazed onto the stainless steel substrate. This type of intermediate layer between the ceramic top layer and the substrate has been shown (ref. 7) to minimize thermally induced stress that could cause YSZ coating spall. Also, because of the porous nature of these fibermetal layers, their thermal conductivity is quite low in comparison with that of a totally dense alloy (ref. 8).

In this series of tests two types of fibermetal[4] were used as an intermediate layer: FM-534 (25Ni-9.0Al-18.5Cr-0.5Co-Fe) and H-875 (22.5Ni-5.5Al-0.5Si-0.1C-Fe). Both materials are about 30 to 35 percent as dense as a totally dense alloy. Both are approximately 0.32 cm (0.125 in.) thick and have a relatively long oxidation life at temperatures below 980 °C (1800 °F).

After fibermetal brazing was completed, the top surface of the fibermetal was grit blasted and plasma sprayed with a thin bond coat. The bond coat was approximately 0.008 to 0.010 cm (0.003 to 0.004 in.) thick and was composed of NiCrAlY (16Cr-6Al-0.14Y-Ni).

The top layer plasma sprayed on the specimen was YSZ that was either 8- or 12-wt% Y_2O_3. This layer was sprayed on in the same manner as the bond coat in thicknesses from 0.15 to 0.20 cm (0.060 to 0.080 in.). All specimens were tested in the as-sprayed condition. Bond coats and ceramic top layers were plasma sprayed by automated equipment. Specimen configurations tested are given in table I.

Test Procedure

The procedure for the sample testing was carried out for the same conditions as used for the rig calibration tests. Specimen and grit material in the test rig were weighed to establish initial conditions. The sample was then placed in the desired downstream location at the desired impingement angle.

Once the rig and specimen were brought to their steady-state conditions (temperatures, pressures, and flow rates), the particle flow was introduced. Figure 4 displays a typical temperature-versus-time plot for the surface, the stainless steel–complaint layer interface, and the substrate back side.

Particle flow was controlled by a commercially available powder feed assembly. Particle flow for any one test lasted typically 2 min. (The mass flow rate of the particles was approximately 0.2 g/sec (1.6 lb/hr) for these tests.)

Once the particle flow for a particular test was completed, the combustor fuel flow was stopped and the rig and sample were allowed to cool to room temperature. Finally the the sample and the grit material were weighed to determine the weight lost by the sample and the amount of grit material used.

This procedure was repeated until either the coating was eroded to the compliant layer or other specimen failures such as spalling of the coating occurred. The number of tests performed on any one sample was a function of impingement angle and distance downstream of the nozzle exit.

Results and Discussion

The high-temperature erosion results presented herein were compiled from 19 different specimens. For material configuration differences between the specimens, see table I. The specimens were tested at three impingement angles (20°, 45°, and 90°) and at three locations downstream of the nozzle exit (7.6, 10.2, and 12.7 cm; 3, 4, and 5 in.).

[4]Brunswick Corporation.

Macroscopic Specimen Evaluation

Specimens were exposed to severe thermal transients because of the starting and stopping of the rig. The surface temperatures of a specimen under the severest starting conditions increased from the ambient temperature of 50 °C (172 °F) to 1500 °C (2732 °F) in approximately 20 seconds. The startup and cooldown cycling caused preferential cracking (mudflat cracks) of the YSZ top layer (fig. 11). This thermally introduced stress relief cracking was found to some degree on all of the specimens tested. The density of these cracks increased as the thermal test environment became more severe.

The crack density was significantly higher at the centerline of the high-temperature gas stream and tended to produce enhanced erosion. Cracks and other surface imperfections subjected to erosion are shown in reference 9 to be zones of increased material removal, for an aluminum alloy tested at low temperatures. The ceramic specimens tested in this study at high temperatures showed the same trends. On specimens positioned at 90° (perpendicular to the flow) both sides of the thermal stress cracks eroded in a similar fashion and at a higher rate than the surrounding surfaces. On specimens positioned at 45° and 20° to the flow the erosive pattern was enhanced downstream of the crack (fig. 12). Also, the specimens were tested in the as-sprayed condition. These as-sprayed surfaces were characterized by some irregularities that were further enhanced and enlarged as the erosive process proceeded, as was seen for the thermal stress cracks.

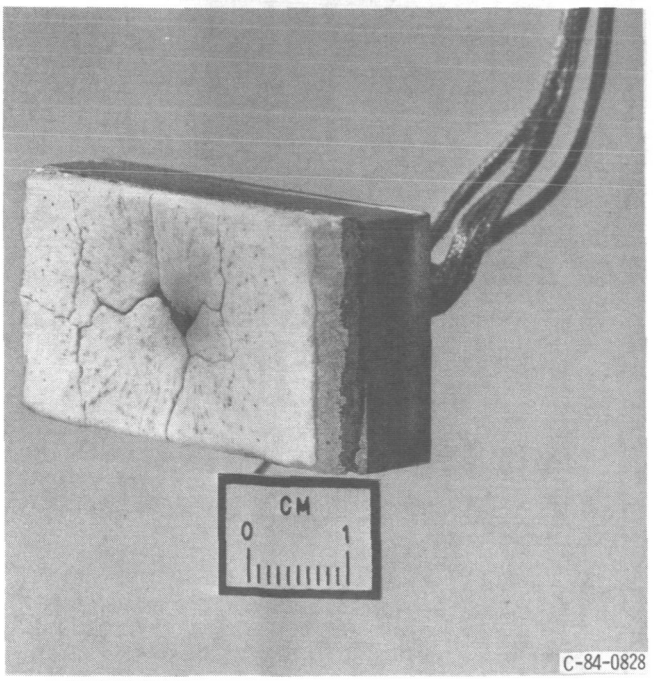

Figure 11.—High-temperature erosion specimen, showing severe mudflat cracks. (Specimen was tested at 7.6 cm (3 in.) downstream of nozzle exit at 90° impingement angle.)

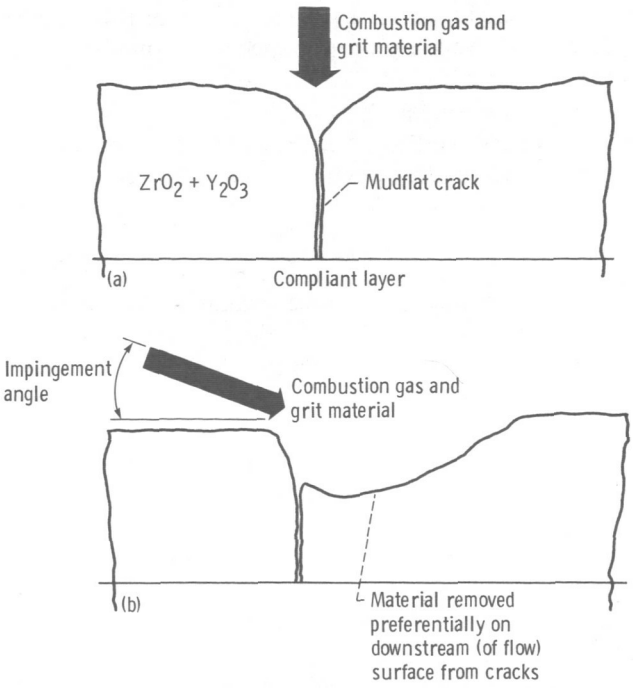

(a) Impingement angle, 90°.
(b) Impingement angle, 45° and 20°.

Figure 12.—Effects of impingement angle on erosion near mudflat-cracked ceramic layer.

Another problem was a leading-edge effect on specimens tested at the shallowest impingement angle. Even though most erosive damage was only slightly off center, the side of the specimen as well as the intended top surface was exposed to the erosive grit. Thus the impingement angle was less well defined, and early failures occurred from cutting into the compliant layer of material caused by grit material impact at near normal trajectory along the leading edge of a small portion of the specimen (fig. 13).

Note that none of the test specimens failed at the compliant layer–substrate interface. Temperatures at this

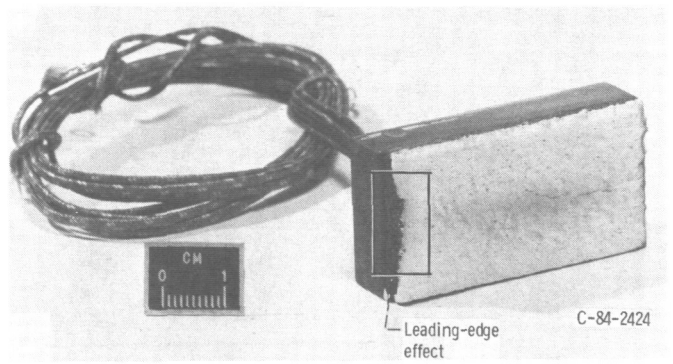

Figure 13.—High-temperature erosion specimen after test at 12.7-cm (5-in.) downstream distance and 20° impingement angle.

location reached nearly 680 °C (1250 °F) for the severest conditions. However, on a few specimens small sections of the top layer did spall off. This usually happened when the top ceramic surface was eroded away and the high-temperature gas and grit were permitted to act on the bond coat layer and through the compliant layer.

Microscopic Specimen Evaluation

Some of the specimens were examined by scanning electron microscope (SEM) to investigate how the surface was affected by the erosive medium. These specimens had typically been cycled from ambient to steady-state temperature and eroded several times. SEM photomicrographs of eroded surfaces were taken at locations where at least 0.76 mm (0.03 in.) of material was worn from the original surface.

The first specimen to be discussed is one in which a series of preliminary surface temperature measurements were made. This particular specimen was not eroded but instead was thermally cycled at a number of downstream positions and perpendicular (90° impingement) to the gas flow. The plasma-sprayed surface (fig. 14) showed microcracking from the plasma spray process along with mudflat cracking due to thermal stress relaxation.

The remaining specimens to be discussed had surfaces that were eroded. Three different specimens (figs. 15 to 17) exposed to the erosive medium at 12.7 and 10.2 cm (5 and 4 in.) downstream of the nozzle exit plane with a 90° impingement angle were examined in the SEM. The surfaces had randomly distributed and oriented markings that indicated particle edge and flat side impacts. Presumably this was caused by the grit material having sharp, well-defined edges (90° typically from one face to the next) along with very flat surfaces between these edges (fig. 6). Also some surface material had been melted and then reattached to nearby surface material (fig. 15).

One specimen examined in the SEM was exposed to the erosive medium 12.7 cm (5 in.) downstream of the nozzle exit plane at a 45° impingement angle. Particle impact sites (fig. 18) were different from those for the 90° impacts. At some impact sites the particle appeared to have penetrated or skidded along the exposed surface. Also found on this particular specimen were areas of material that had no surface damage (fig. 19).

The last specimen studied by SEM was exposed to the hot gas and erosive medium at 12.7 cm (5 in.) downstream of the nozzle exit at a 20° impingement angle. The type of posterosion surface found here was particle-

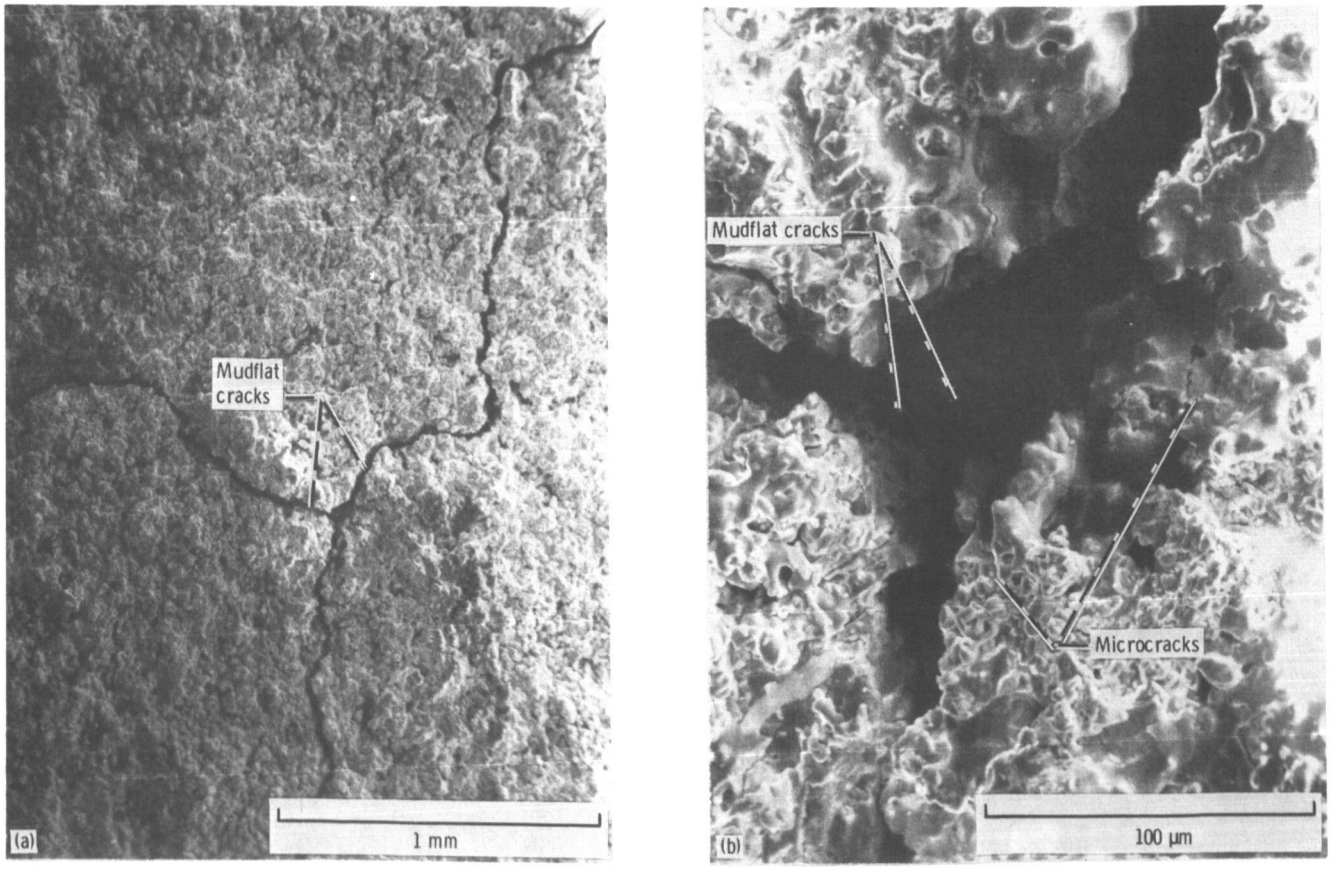

Figure 14.—Specimen 9a after rig test without erosive particles in flow, showing mudflat cracks and microcracking of YSZ.

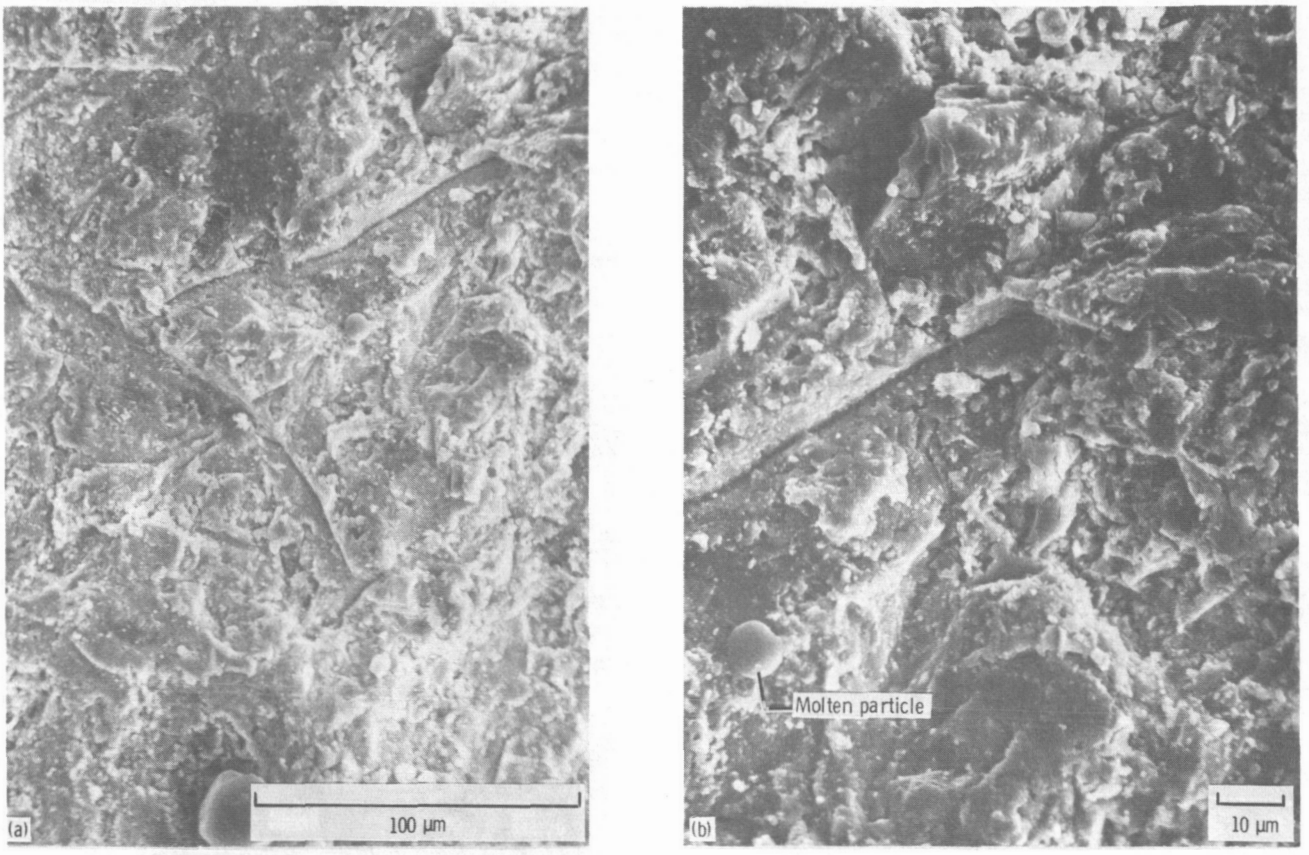

(a) Randomly oriented edge impacts.
(b) Molten material of surface near an impact mark (closeup of fig. 15(a)).

Figure 15.—Specimen 24 eroded at 12.7-cm (5-in.) downstream distance and 90° impingement angle.

corner "machining" marks (fig. 20, top left photograph). Two higher magnification SEM photographs of an impact location from the YSZ specimen are also shown in figure 20.

The SEM photographs indicate that the posterosion surface differs depending on the impingement angle. Directly perpendicular impingement caused a continuous zone of damage. At 45° impingement the posterosion surface appeared to have particle "skid" marks. At 45° and 20° some surface areas had no apparent damage even though 0.08 cm (0.03 in.) of YSZ had been eroded above these locations. At 20° impingement particle indentations appeared as machining marks and were presumably caused by the edges of the particle corners interacting with the YSZ surface. Surface impact locations for all of the specimens showed that plastic deformation had occurred at least on a microscopic scale.

Measured Erosion Rates

In this series of tests YSZ specimen performance was determined by weight loss. The ceramic specimens typically were subjected to multiple tests. The weight change of the specimen and the amount of grit material used were checked after each erosion test. Before the test was resumed, the surface of the specimen was visually inspected to ensure that it would survive the next test.

At least two different specimens were tested at each location and impingement angle, except at the severest location and conditions—7.6 cm (3 in.) and perpendicular to the flow—where only one specimen was tested. In the data taken from the post-test weighings (fig. 21) the first trend to note is that for the three downstream locations investigated at constant impingement angle the slopes of the curves for weight lost versus particulate spent are similar. Thus the surface temperature during erosion (1150 to 1500 °C; 2100 to 2730 °F), the particle velocity (260 to 320 m/s; 850 to 1050 ft/s), and the particle diffusion pattern, which changed with location in the flow, did not significantly affect the bulk erosion rate at constant impingement angle. Note also that differences in the compositions of the YSZ and the compliant layer had no effect on the bulk erosion rate.

However, the time (or amount of grit material used) to specimen failure was affected by impingement angle. On the basis of the concentration of grit material in the flow, shallow impingement angles resulted in wear spread over

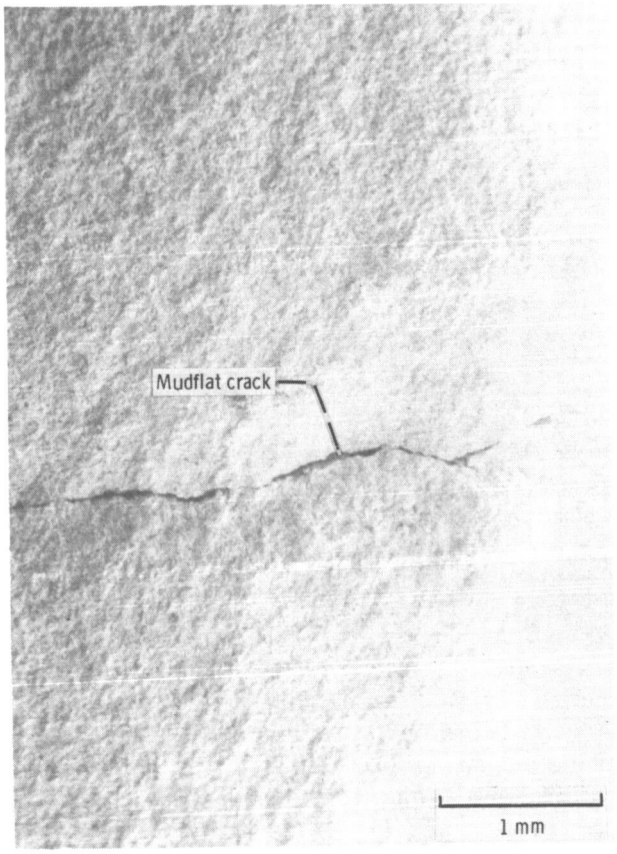

Figure 16.—SEM photograph showing preferential erosion in zone near mudflat crack. Specimen eroded at 12.7-cm (5-in.) downstream distance and 90° impingement angle.

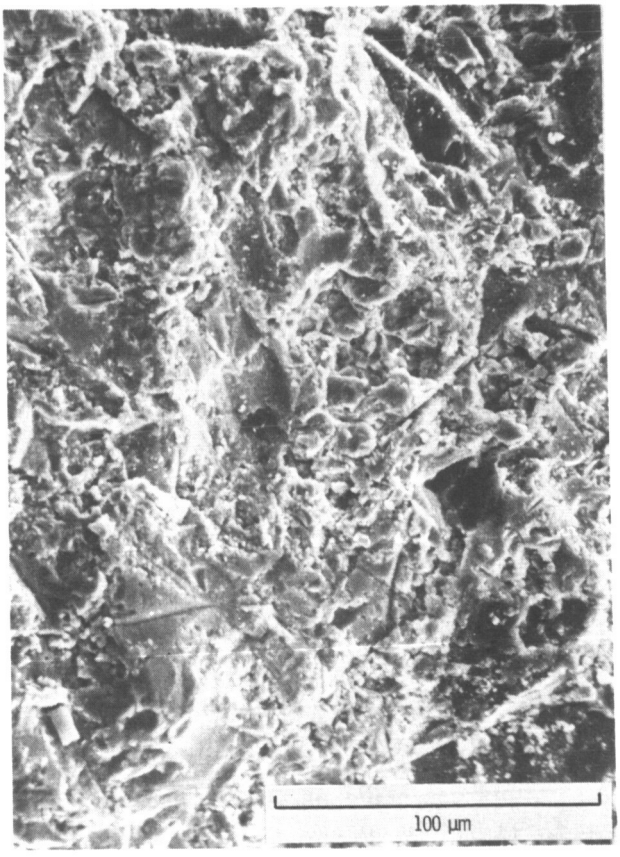

Figure 17.—SEM photograph showing surface damage in region 0.076 cm (0.030 in.) below initial untested surface before tests were conducted at 10.2-cm (4-in.) downstream distance and 90° impingement angle.

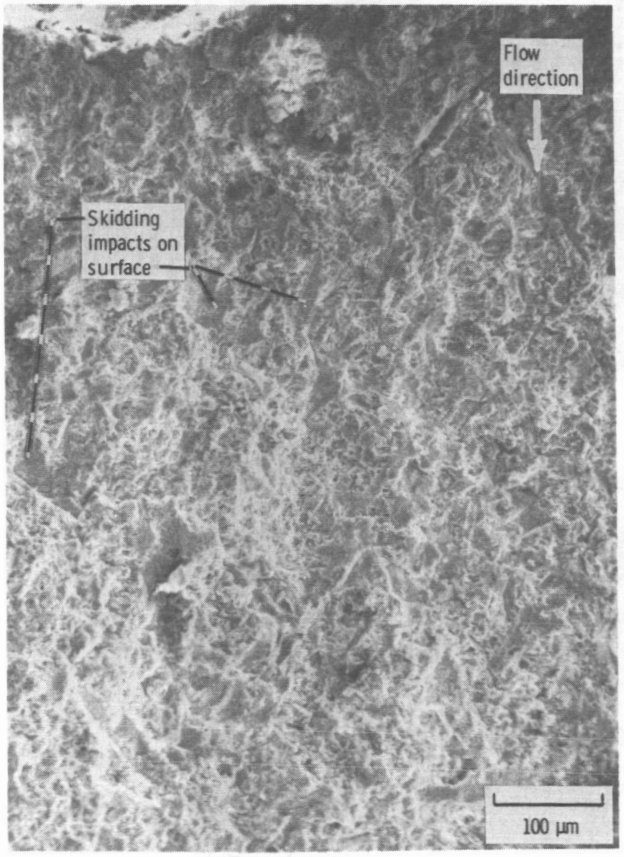

Figure 18.—SEM photograph of specimen 7, which was eroded at 12.7-cm (5-in.) downstream distance and 45° impingement angle, showing "skidding" impacts on surface.

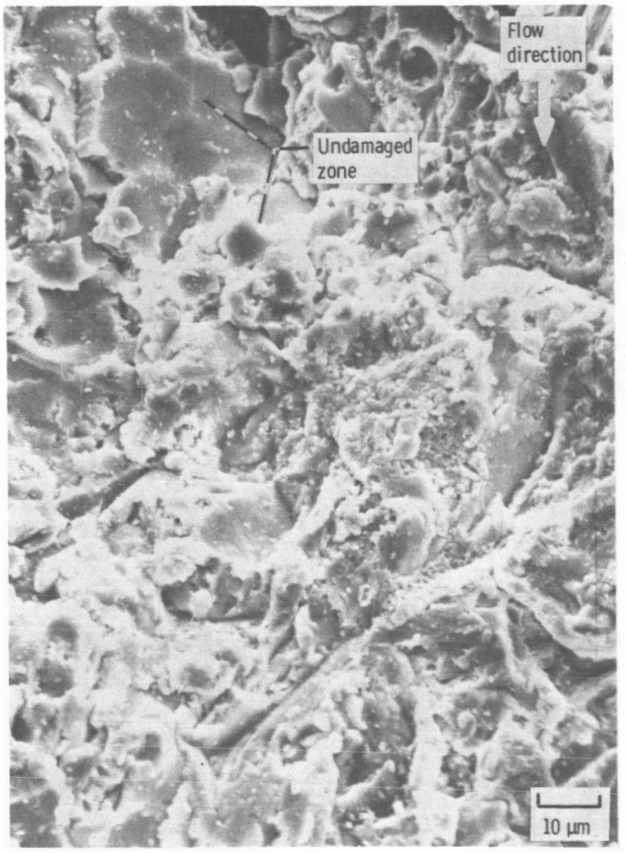

Figure 19.—SEM photograph showing zone of undamaged material. (Location of zone is where approximately 0.10 cm (0.04 in.) of YSZ was eroded to expose this region.)

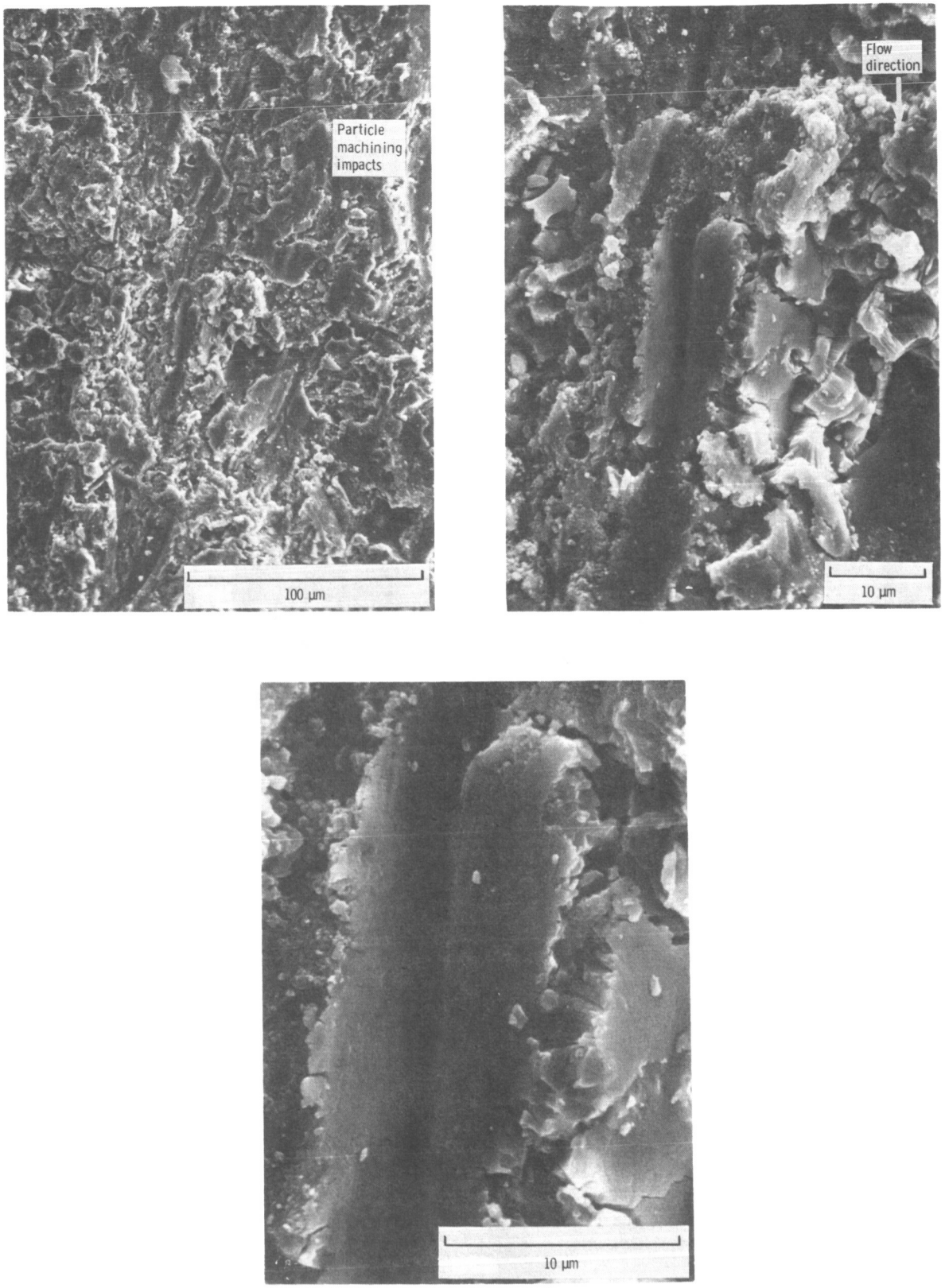

Figure 20.—SEM photographs of specimen 6a, which was eroded at 12.7-cm (5-in.) downstream distance and 20° impingement angle, showing eroded YSZ surface at different magnifications.

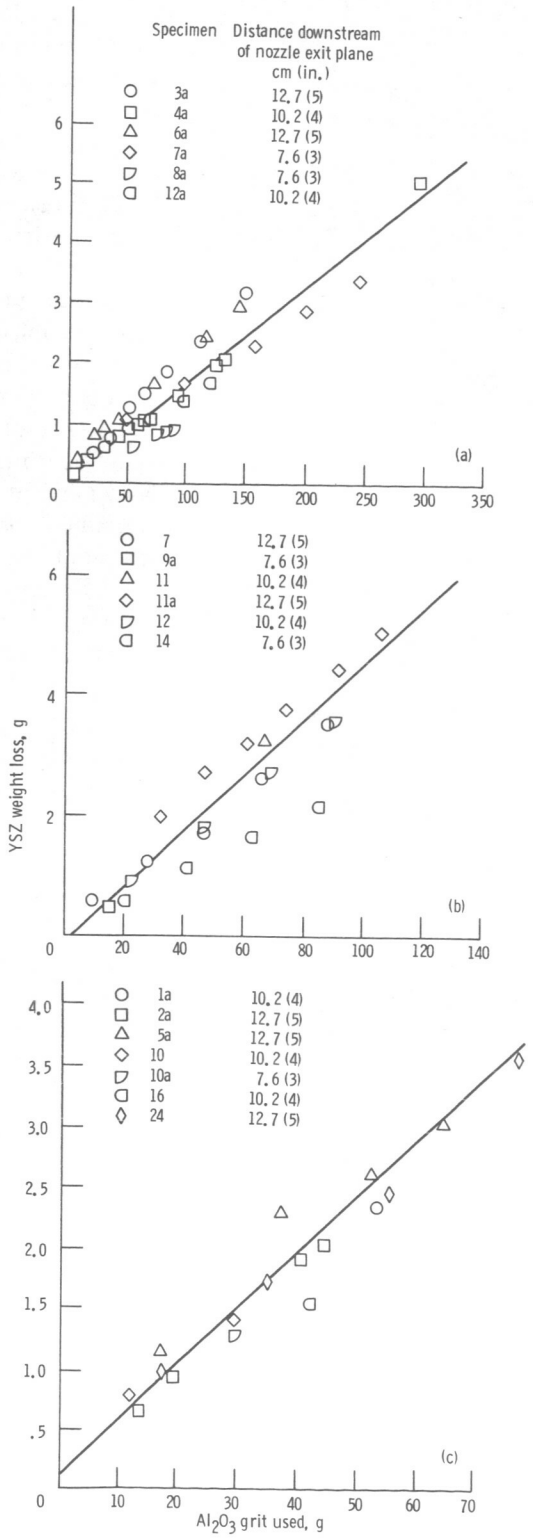

(a) Impingement angle, 20°. YSZ weight lost (g) = 0.0151 (Al_2O_3 grit used) + 0.209.
(b) Impingement angle, 45°. YSZ weight lost (g) = 0.044 (Al_2O_3 grit used) − 0.12.
(c) Impingement angle, 90°. YSZ weight lost (g) = 0.0465 (Al_2O_3 grit used) + 0.098.

Figure 21.—YSZ weight loss as a function of impingement angle.

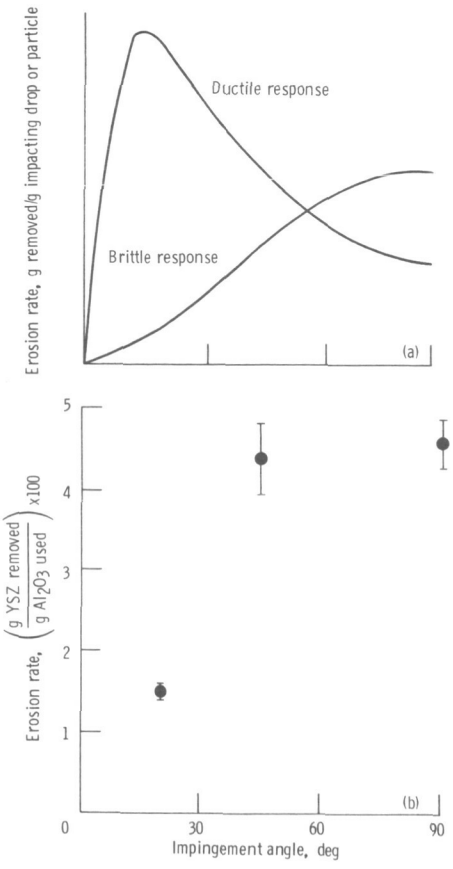

(a) Ductile and brittle material erosion response. (From ref. 10.)
(b) YSZ specimen. Error bars denote ±1 standard deviation on slope.

Figure 22.—Erosion rate as a function of impingement angle for YSZ specimen, compared with curves for ductile and brittle materials.

a larger surface area. This allowed the shallow-angled specimen to continue in the testing phase longer (fig. 21). Also, the normal component of particle velocity (or the energy available for surface deformation) diminished with shallower impingement angles.

Typical behavior of ductile and brittle materials to solid-particle erosion is shown in figure 22(a). The angular dependence of erosion rate (slope of weight loss curves) for the YSZ tested is shown in figure 22(b). The data, though limited to these points, are more representative of brittle material than of ductile materials, which tend to have their highest erosion rates at approximately 20° (ref. 10). In this investigation the lowest erosion rate occurred at this impingement angle.

In summary, the plasma-sprayed YSZ studied herein deformed plastically (ductile behavior), as observed microscopically, but its overall erosion rate was representative of a brittle material.

Summary of Results

The data accumulated in this series of tests on plasma-sprayed yttria-stabilized zirconia gas path seals indicated the following results:

1. Material removal was slower at shallow impingement angles (20°) than at 45° and 90°.

2. Microscopic evaluation of specimen surfaces indicated plastic deformation (ductile behavior), but material overall erosion behavior suggested brittle material erosion rates.

3. Erosion activity was greater at cracks, surface imperfections, and other sources of surface irregularities. The surfaces changed in appearance depending on the impingement angle of exposure on both microscopic and macroscopic scales.

4. Sample differences in weight percentage of Y_2O_3 and compliant layer material did not have any effect on erosion results.

5. Specimen surface temperature, particle velocity, and particle diffusion in the flow, which changes with specimen location, did not alter bulk erosion rate at constant impingement angle.

6. Severe thermal transients from the heating and cooling cycles produced mudflat cracks in all of the specimens tested.

National Aeronautics and Space Administration
Lewis Research Center
Cleveland, Ohio, September 18, 1984

References

1. Ludwig, Lawrence P.; and Bill, Robert C.: Gas Path Sealing in Turbine Engines. ASLE Trans., vol. 23, no. 1, Jan. 1980, pp.1-22.
2. Tabakoff, W.; and Wakeman, T.: Test Facility for Material Erosion at High Temperature. Erosion: Prevention and Useful Applications, ASTM-STP-664, W.F. Adler, ed., American Society for Testing and Materials, 1979, pp. 123-135.
3. Liebert, Curt H.: Emittance and Absorptance of NASA Ceramic Thermal Barrier Coating System. NASA TP-1190, 1978.
4. Tabakoff, W.; Hamed, A.; and Beacher, B.: Investigation of Gas Particle Flow in an Erosion Wind Tunnel. Wear, vol. 86, no. 1, Apr. 1, 1983, pp. 73-88.
5. Ponnaganti, V.; Stock, D.E.; and Sheldon, G.L.: Measurement of Particle Velocities in Erosion Processes. Polyphase Flow and Transport Technology, R.A. Bajura, ed., American Society of Mechanical Engineers, 1980, pp. 217-222.
6. Ruff, A.W.; and Ives, L.K.: Measurement of Solid Particle Velocity in Erosive Wear. Wear, vol. 35, 1975, pp.195-199.
7. Bill, Robert C.; and Wisander, Donald W.: Preliminary Study of Cyclic Thermal Shock Resistance of Plasma Sprayed Zirconium Oxide Turbine Outer Air Seal Shrouds. NASA TM-73852, 1977.
8. Tolokan, R.P.; and Nablo, J.C.: High Temperature Ceramic Metal Attachment Using a Strain Absorbing Fiber Metal Pad. SAMPE Quarterly, vol. 12, no. 3, Apr. 1981, pp. 1-7.
9. Rao, P.Veerabhadra; and Buckley, Donald H.: Solid Particle Impingement Erosion Characteristics of Cylindrical Surfaces, Preexisting Holes, and Slits. NASA TM-83322, 1983.
10. Schmitt, George F.: Liquid and Solid Particle Impact Erosion. Wear Control Handbook, M.B. Peterson and W.O. Winer, eds., 1980, pp. 231-282.

1. Report No. NASA TP-2406 AVSCOM TR 84-C-17	2. Government Accession No.	3. Recipient's Catalog No.

4. Title and Subtitle	5. Report Date
High-Temperature Erosion of Plasma-Sprayed, Yttria-Stabilized Zirconia in a Simulated Turbine Environment	December 1984
	6. Performing Organization Code 505-33-52
7. Author(s) Robert F. Handschuh	8. Performing Organization Report No. E-2271
	10. Work Unit No.
9. Performing Organization Name and Address NASA Lewis Research Center and Propulsion Laboratory U.S. Army Research and Technology Laboratories (AVSCOM) Cleveland, Ohio 44135	11. Contract or Grant No.
	13. Type of Report and Period Covered Technical Paper
12. Sponsoring Agency Name and Address National Aeronautics and Space Administration Washington, D.C. 20546 and U.S. Army Aviation Systems Command, St. Louis, Mo. 63120	14. Sponsoring Agency Code

15. Supplementary Notes

Robert F. Handschuh, Propulsion Laboratory, U.S. Army Research and Technology Laboratories (AVSCOM)

16. Abstract

A series of rig calibration and high-temperature tests simulating gas path seal erosion in turbine engines were performed at three impingement angles and at three downstream locations. Plasma-sprayed, yttria-stabilized zirconia specimens were tested. Steady-state erosion curves presented for 19 test specimens indicate a brittle type of material erosion despite scanning electron microscopy evidence of plastic deformation. Steady-state erosion results were not sensitive to downstream location but were sensitive to impingement angle. At different downstream locations specimen surface temperature varied from 1250 to 1600 ^{o}C (2280 to 2900 ^{o}F) and particle velocity varied from 260 to 320 m/s (850 to 1050 ft/s). The mass ratio of combustion products to erosive grit material was typically 240.

17. Key Words (Suggested by Author(s))

High-temperature erosion
Gas turbine seals
Plasma-sprayed zirconia
Solid particle impingement

18. Distribution Statement

Unclassified - unlimited
STAR Category 27

19. Security Classif. (of this report)	20. Security Classif. (of this page)	21. No. of pages	22. Price*
Unclassified	Unclassified	18	A02

*For sale by the National Technical Information Service, Springfield, Virginia 22161

8 2 1U,C, 841207 S00161DS
DEPT OF THE AIR FORCE
ARNOLD ENG DEVELOPMENT CENTER(AFSC)
ATTN: LIBRARY/DOCUMENTS
ARNOLD AF STA TN 37389